ELSEVIER

Journal of Nuclear Materials 298 (2001) 329–339

journal of nuclear materials

www.elsevier.com/locate/jnucmat

Torsion texture development of zirconium alloys

P. Sanchez [a], A. Pochettino [a,b,*], T. Chauveau [c], B. Bacroix [c]

[a] *Escuela de Posgrado, Universidad Nacional de General San Martín, Belgrano 3563, 1650 San Martín, Argentina*
[b] *Dpto. Materiales, CAC, Comisión Nacional de Energía Atómica, Av. Libertador 8250, 1429 Buenos Aires, Argentina*
[c] *LPMTM-CNRS, Université Paris 13, 99 Av.J.B. Clément, 93430 Villetaneuse, France*

Received 29 December 2000; accepted 23 May 2001

Abstract

In order to study texture formation during high temperature torsion tests of Zirconium alloys, results from experiments and simulations are presented and compared in this paper. Simulations put in evidence that the Viscoplastic Selfconsistent model (VPSC), in spite of some limitations for the description of plastic deformation at high temperatures, gives a reasonable description of the experimental textures. Predictions show that prismatic and basal $\langle a \rangle$ slip are necessary to reproduce the main texture components and that pyramidal $\langle c + a \rangle$ slip must have a low activity.

PACS: 62.20.Fe; 81.20.Hy; 81.40.Lm

1. Introduction

Torsion tests are technologically important because they are often used at the industrial level to simulate high temperature deformation processes (e.g., rolling, forging, and extrusion) or to assess the hot working properties of steels and other metallic alloys [1]. In the case of cubic metals, many investigations concerning texture and materials properties evolution under hot torsion tests were performed. In particular, many comparisons between experiments and simulations of texture evolution during torsion can be found in the literature. For cubic face centered materials (fcc), Van Houtte [2] was the first to use the Taylor Model in order to simulate and interpret both rolling and torsion textures for a wide variety of stacking fault energies. By adding twinning to the more classical slip mode as a possible deformation mechanism for low stacking fault energy materials, the so-called Copper and Brass textures were obtained. Later, Canova et al. [3] showed that the introduction of the relaxed conditions in the Taylor Model, allows a better description of torsion texture development for high strains. The effect of temperature on the evolution of torsion textures was also studied by various authors [4–6] for fcc metals. By contrast, much less is known about torsion texture development in body centered materials (bcc). In these materials, few experimental data concerning α-Fe are reported [7,8] and more recently texture development during room temperature torsion tests of a Ti–Nb IF Steel was studied experimentally as well as theoretically [9].

Another interesting feature of torsion tests is the phenomenon of lengthening, which can takes place in fcc and bcc polycrystalline materials, depending on the initial texture. This phenomenon is related to axial stresses induced during the torsion test and was first discussed by Swift in 1947 [10]. Later on, several experimental and theoretical studies were developed to understand the physical origin of this lengthening [11,12]. It was thus shown that induced axial stresses are generally compressive at low temperatures and small strains and they drop to small compressive values (Al) or become tensile (Cu and α-Fe) when temperature and strain are increased. These papers also clearly showed that there was a strong correlation between the axial stresses and the major texture components.

* Corresponding author. Tel.: +54-11 4754 7250; fax: +54-11 4754 7383.
E-mail address: pochett@cnea.gov.ar (A. Pochettino).

0022-3115/01/$ - see front matter
PII: S0022-3115(01)00640-7

In contrast to the situation concerning cubic materials, nothing is said in the literature about torsion tests on hexagonal closed packed materials, in spite of the wide use of titanium and zirconium alloys in chemistry, aeronautical and nuclear industries. These alloys are already well known for their good mechanical properties, especially at room temperature, their excellent resistance to corrosion and – in the case of Zr for nuclear industry – their low cross-section for neutron capture. But few studies concern the behavior of these alloys at elevated temperatures and high strains.

Zirconium alloys present anisotropic elastic, plastic, thermal and irradiation properties at the single crystal level. In polycrystals, these properties are strongly affected by the existence of crystallographic textures, and this is why the knowledge of texture and of its effects on the mechanical behavior of zirconium alloys is of technological importance. In the case of rolling processes, the texture evolution in Zr alloys has been studied at room and high temperature [13–15]. The experimental data have been compared with simulations performed using the Viscoplastic Selfconsistent model (VPSC). In order to obtain an accurate representation of rolling textures at different temperatures, a systematic analysis of the active deformation modes as well their critical resolved shear stress (CRSS) dependence with temperature was carried out. CRSS values were chosen within the ranges reported in the literature to assure the best agreement with experiments.

In order to extend the study of texture formation in Zr alloys under different deformation processes, results from experiments and simulations for torsion tests of Zircaloy-4 samples at high temperature ($T = 750$ °C) are presented in the present paper. Similarly to previous studies, predictions of torsion textures are performed using the VPSC model and the activation of different deformation modes and their effect on texture development are also analyzed.

2. Experimental procedure

Torsion test samples were obtained from cylindrical rods of Zry-4 (1.5% Sn, 0.21% Fe, 0.10% Cr, 0.01% O) which were machined to a diameter of 8 mm and a gauge length of 12 mm. Fixed end torsion tests (i.e., the sample length remains constant during straining) were performed for two true strains: $\varepsilon = 0.8$ and $\varepsilon = 1.8$ (with a deformation rate of 1 s^{-1}). The tests were carried out at a temperature equal to 750 °C. The sense of the torsion shear strain, which was the same for all the torsion experiments, is indicated in Fig. 1; according to previous works [6], the used convention corresponds to *negative* shearing. Equivalent stress–strain curves obtained from the torsion tests show that for equivalent strains greater than $\varepsilon = 0.3$, the stress does not evolve with strain, indicating the presence of a steady state region. This result indicates that the material undergoes some dynamic recovery.

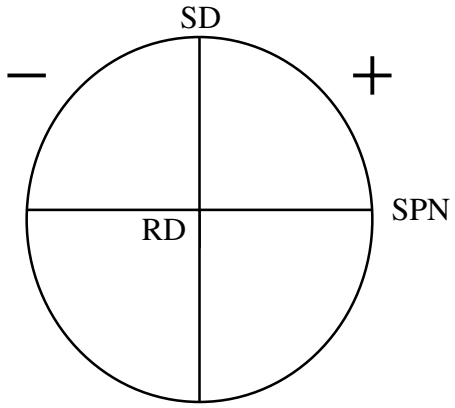

Fig. 1. Definition of principal reference axes for torsion tests in rods: SPN direction, SD and RD.

Experimental information about texture was obtained by using conventional X-rays diffraction techniques. Incomplete $\{0002\}$, $\{10\bar{1}0\}$ and $\{10\bar{1}1\}$ pole figures were obtained using the reflection method and texture analysis was performed using the orientation distribution function (ODF) description given by both Harmonic Method developed by Bunge [16] and Vector Method developed by Vadon [17].

3. Experimental textures

Pole figures are plotted on the plane defined by the axial direction (Z) of the rods, which is also the normal to the shear plane in torsion experiments (SPN), and the shear direction (SD), the radial direction (RD) of samples being perpendicular to this axis (Fig. 1). The sample and crystal reference systems, which need to be defined for the analysis of texture, are thus (SPN, SD, RD) and $(10\bar{1}0, 11\bar{2}0, 0001)$, respectively. Accounting for both crystal (hexagonal) and process (centro-symmetry from torsion) symmetries, the Euler angles (ϕ_1, ϕ, ϕ_2), which define the rotation from the sample reference system to the crystal reference system, can be varied in the reduced Euler space [0°, 180°], [0°, 90°], [0°, 60°] [16].

The stereographic projection plane (SPN-SD) can be divided into four quadrants. Considering the sense of rotations induced by the torsion tests as well as the used conventions for representation, the upper right and the lower left quadrants of the pole figures represented in this work can be considered as extension quadrants. The direction of greatest extension rate being initially placed at 45° from the SPN axis is labeled with the sign (+) in the figures. The other quadrants can be considered as compression quadrants and the direction associated to

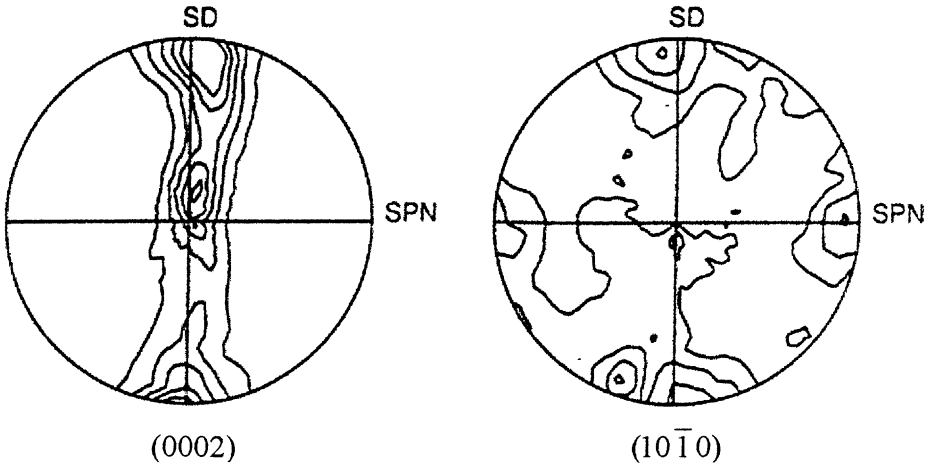

Fig. 2. Experimental pole figures (0002) and (10$\bar{1}$0) for the initial state of the Zircaloy-4 rod.

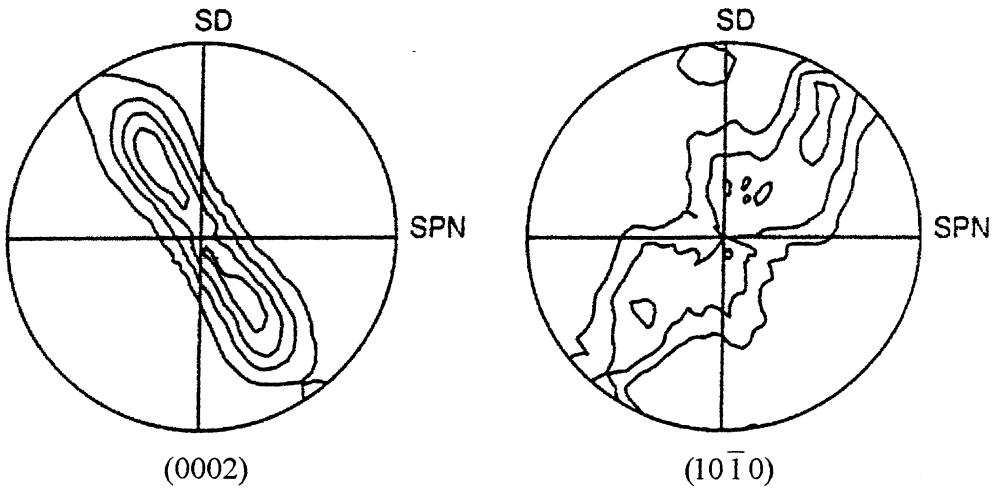

Fig. 3. Experimental pole figures (0002) and (10$\bar{1}$0) after a high temperature torsion test (750 °C) for an effective deformation $\varepsilon = 0.8$.

the greatest compression rate is labeled with the sign (−) (Fig. 1) [18].

Figs. 2–4 show the $\{0002\}$ and $\{10\bar{1}0\}$ pole figures corresponding to the textures measured on the initial state and after torsion tests performed at the two strains of $\varepsilon = 0.8$ and $\varepsilon = 1.8$. The associated ODFs are presented in Figs. 5–7. Figures are plotted using lines of isodensity 1.

In the case of the initial sample, the main texture component is a fiber texture around the axial axis, which is parallel to a $\langle 10\bar{1}0\rangle$ direction and a more or less uniform distribution of $\{0002\}$ poles in the (RD, SD) plane. This $\{10\bar{1}0\}\langle$uvtw$\rangle$ [1] fiber is described by the Euler angles $(0°, \phi, 0°)$ (or equivalently $(0°, \phi, 60°)$) and the maximum intensity is found for $(0°, 90°, 0°)$, which corresponds to the orientation $\langle 0001\rangle$. A minor component $\{11\bar{2}0\}\langle 10\bar{1}0\rangle$ is also visible on the pole figures, which corresponds to the Euler angles $(0°, 0°, 0°)$ (the radial direction is then parallel to the $\langle c\rangle$ axis).

The $\{0002\}$ and $\{10\bar{1}0\}$ pole figures for the deformed samples show that the main texture component is also an approximate fiber whose axis is still located in the (SD, SPN) plane. It rotates roughly from the axial direction towards the (+) direction with increasing strain (i.e., the rotation is in the sense of shear, as expected [6]). For a true strain of $\varepsilon = 0.8$, the distribution of $\langle c\rangle$ axes presents two reinforcements located at ~30°–40° from the radial direction (Fig. 3(a)). For the strain of $\varepsilon = 1.8$, the principal reinforcement is clearly around the radial direction (Fig. 4(a)).

[1] For torsion, {hkil} represent the Miller indices of the shear plane normal and ⟨uvtw⟩ those of the SD.

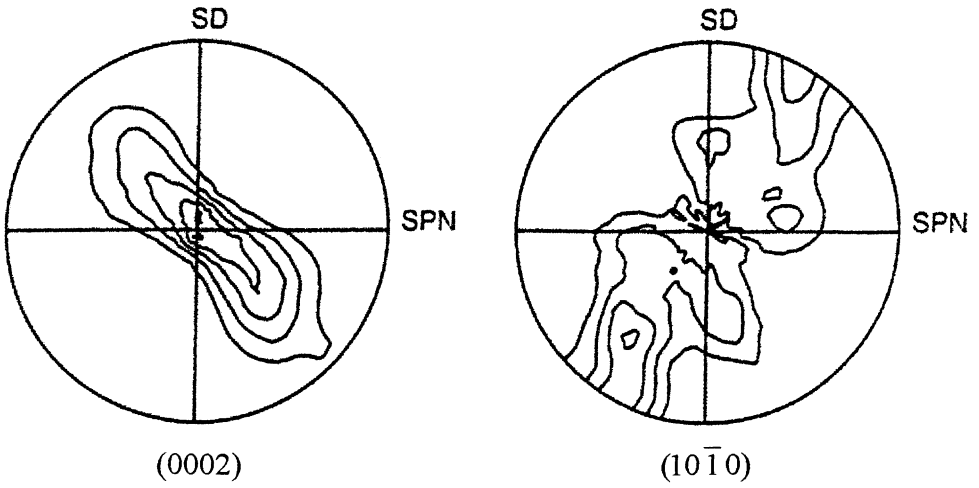

Fig. 4. Experimental pole figures (0002) and (10$\bar{1}$0) after a high temperature torsion test for an effective deformation $\varepsilon = 1.8$.

The analysis of the ODF indicates that this rotated fiber can be described by the following triplets of Euler angles: (30°, ϕ, 20°) for the strain of 0.8 and (60°, ϕ, 0°) for the strain of 1.8. For these two cases, some reinforcements are found along the fibers at (30°, 30°, 20°) and (60°, 0°, 0°), respectively. By using the equivalent description of orientations, it can thus be concluded that the initial fiber component developed during rolling transforms during torsion as follows:

$$(0°, \phi, 60°) \text{ at } \varepsilon = 0 \quad \Rightarrow \quad (30°, \phi, 20°) \text{ at } \varepsilon = 0.8 \quad \Rightarrow \quad (60°, \phi, 0°) \text{ at } \varepsilon = 1.8.$$

On the {0002} pole figure, ϕ_1 corresponds to the angle between the SPN axis and the axis of the fiber, whereas ϕ defines the angle between the radial direction and the $\langle c \rangle$ axis of a given orientation. During negative torsion, it is well known that an overall anti-clockwise rotation of textures is usually observed [6], associated in this case with an increase of ϕ_1. At the same time, the reinforcements of the $\langle c \rangle$ axes along the rotating fiber go from an outside position ($\phi = 90°$) at zero strain towards a central one ($\phi = 0°$) at the maximum strain.

It is finally of interest to note that the overall rotation measured at $\varepsilon = 1.8 (\phi_1 = 60°)$ corresponds exactly to the orientation of the so-called *rotationless* frame used in continuum mechanics [19]. This frame rotates with the principal axes of strain and its final position is equal to $\mathrm{tg}^{-1}(\gamma/2) = 57.3°$. Moreover, it has been shown that this frame was close to the one in which the loss of orthotropy is minimized [20]. It is somewhat surprising that these observations are made for various temperatures as well, i.e., both at room [20] and high temperature (present work). This would then tends to indicate that the rotation rate (i.e., the rate of evolution of texture) is not so much affected by the test temperature.

There remains now to interpret the observed texture evolution, and in particular to deduce from a comparison with predicted textures, the influence of the temperature of the test. This is the aim of the following section.

4. Torsion texture predictions

4.1. Details of the calculation

Torsion texture evolution was predicted using the well-known 1-site VPSC model [21]. This model allows each grain to deform differently, depending on the strength of the interaction between the grain and its surroundings. A viscoplastic constitutive equation is assumed for the grain (associated to a single crystal):

$$\dot{\varepsilon} = \gamma_0 \sum_s m^s \left(\frac{m^s \sigma}{\tau_c^s} \right)^n, \tag{1}$$

where $\dot{\varepsilon}$ and σ are the local strain rate and deviatoric stress, respectively, s identifies the active deformation systems, m^s is the Schmid tensor, τ_c^s is the CRSS of each system, n is the inverse of the rate sensitivity and γ_0 is a scaling factor. Micro and macro magnitudes are related through the interaction equation:

$$\dot{\varepsilon} - \dot{E} = -\tilde{M}(\sigma - \Sigma), \tag{2}$$

where $\tilde{M}$ is the interaction tensor that must be calculated in a selfconsistent way.

It was pointed out before that possible dynamic recovery effects are observed during torsion tests. As it is well known, dynamic recovery allows dislocations, which glide on a given slip plane, to climb from pile-ups and to resume gliding on the same slip system as

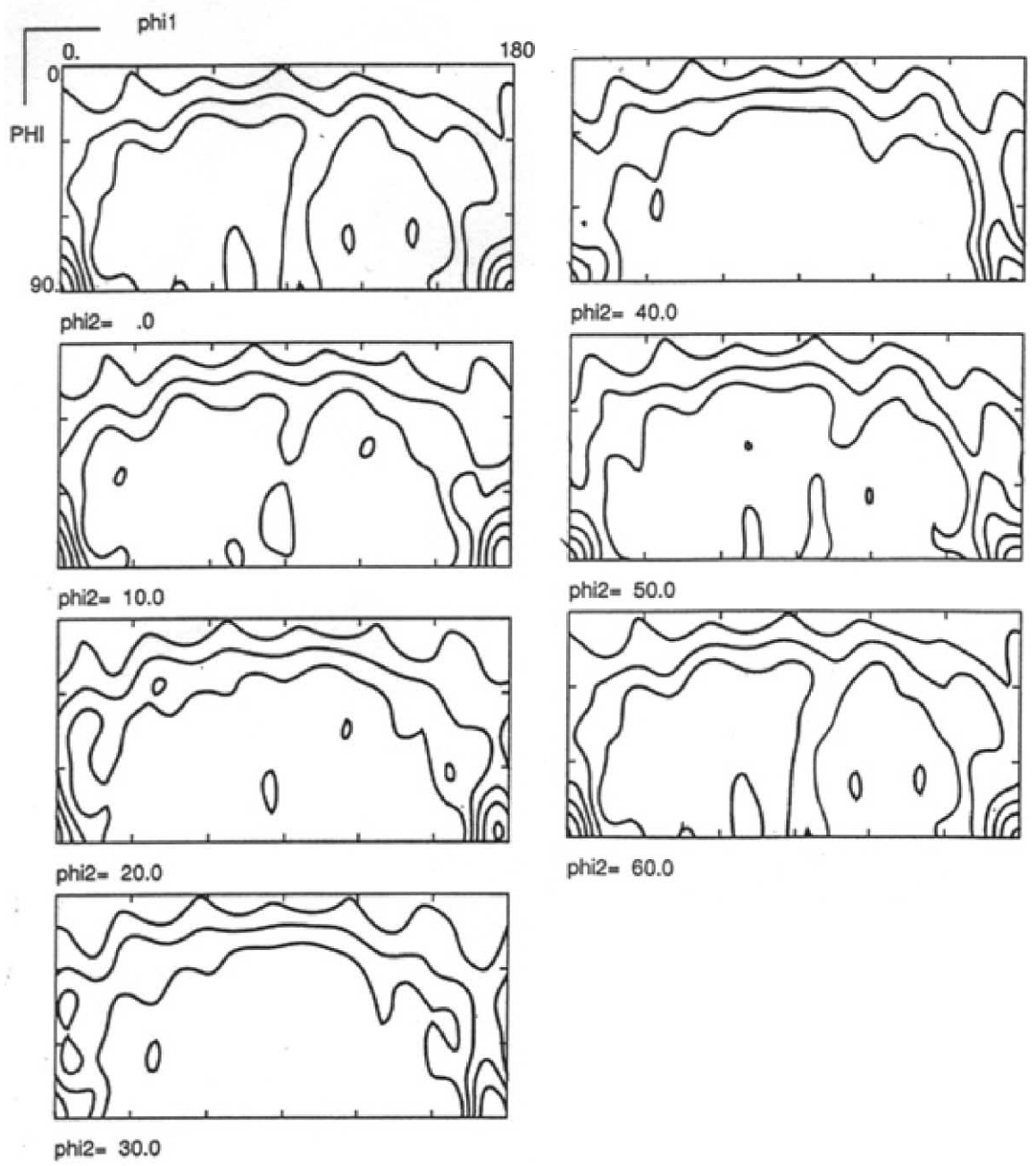

Fig. 5. ODF for the Zircaloy-4 rod at the initial state.

previously. This phenomenon, which is thermally activated, facilitates the accommodation of plastic deformation in grains. In order to approximately account for this fact, a viscoplastic coefficient value of $n = 7$ was used in the single crystal constitutive equation (Eq. (1)). This value is lower than the coefficient used in room temperature simulations of texture development in hcp materials (typically $n = 19$) and it implies a higher strain rate sensitivity for plasticity in grains [22].

The effect of the possible deformation modes on torsion texture development was analyzed in order to understand their effects on final textures. This was done by predictions of torsion textures using each deformation mode separately ($\varepsilon = 0.8$). The initial texture corresponds to a random distribution of orientations and

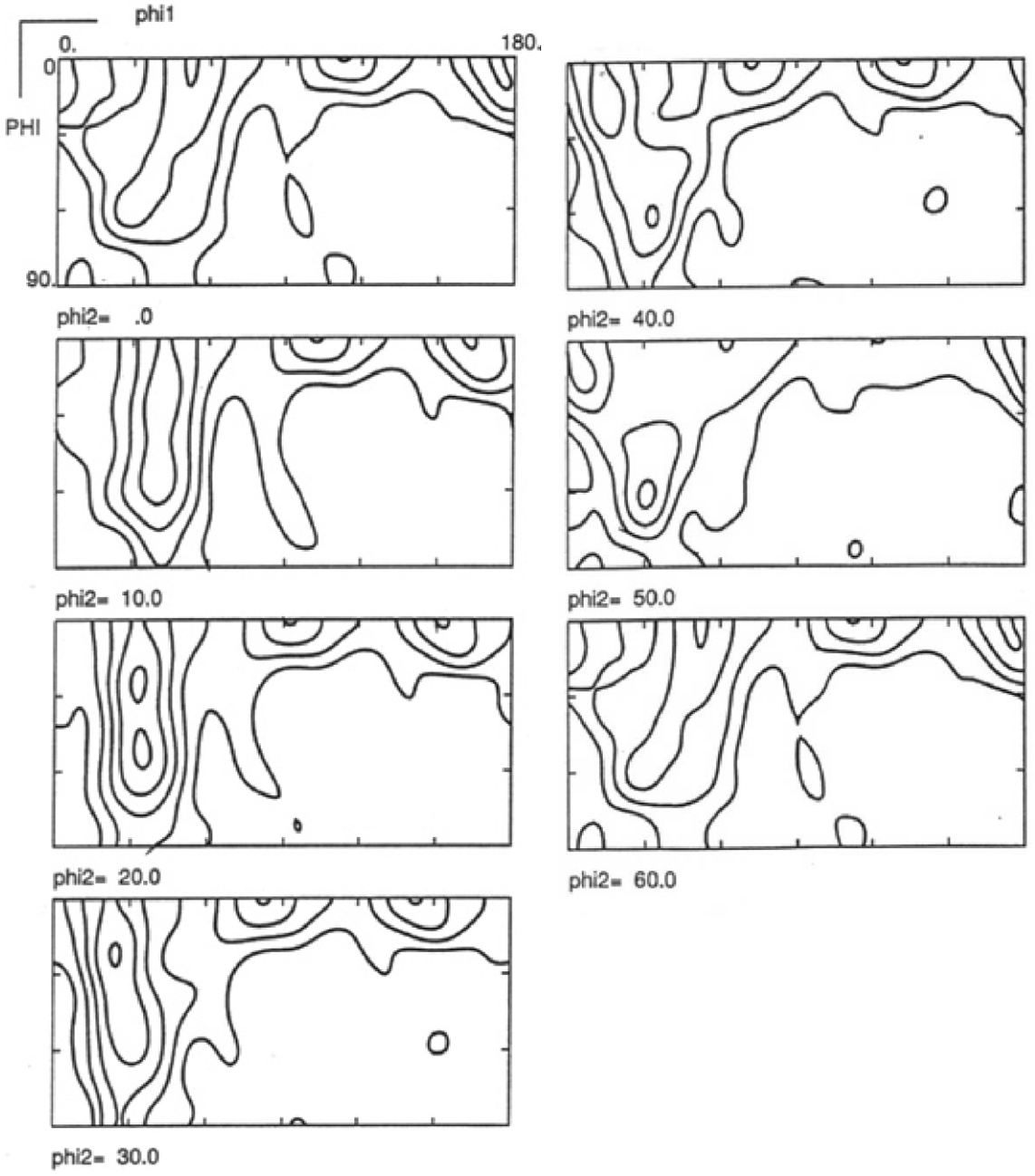

Fig. 6. ODF after a high temperature torsion test ($\varepsilon = 0.8$).

the results are presented in Fig. 8, in the form of (0 0 0 2) pole figures. Pole densities are plotted using lines of isodensity 1 and dots correspond to regions presenting values lower than 1.

Fig. 8(a) shows the effect of prismatic slip. This deformation mode generates a distribution of (0 0 0 2) poles presenting an approximate fiber distribution around the direction of greatest contraction. Pole densities present a maximum value around the radial direction. Basal slip (Fig. 8(b)) produce a well-defined maximum on the (0 0 0 2) pole density distribution placed over the stereographic circle at the greatest contraction direction. For high deformations, these pole reinforcements rotate and a strong concentration of $\langle c \rangle$ axes around SPN can be observed. The reorientation introduced by the activity of the pyramidal

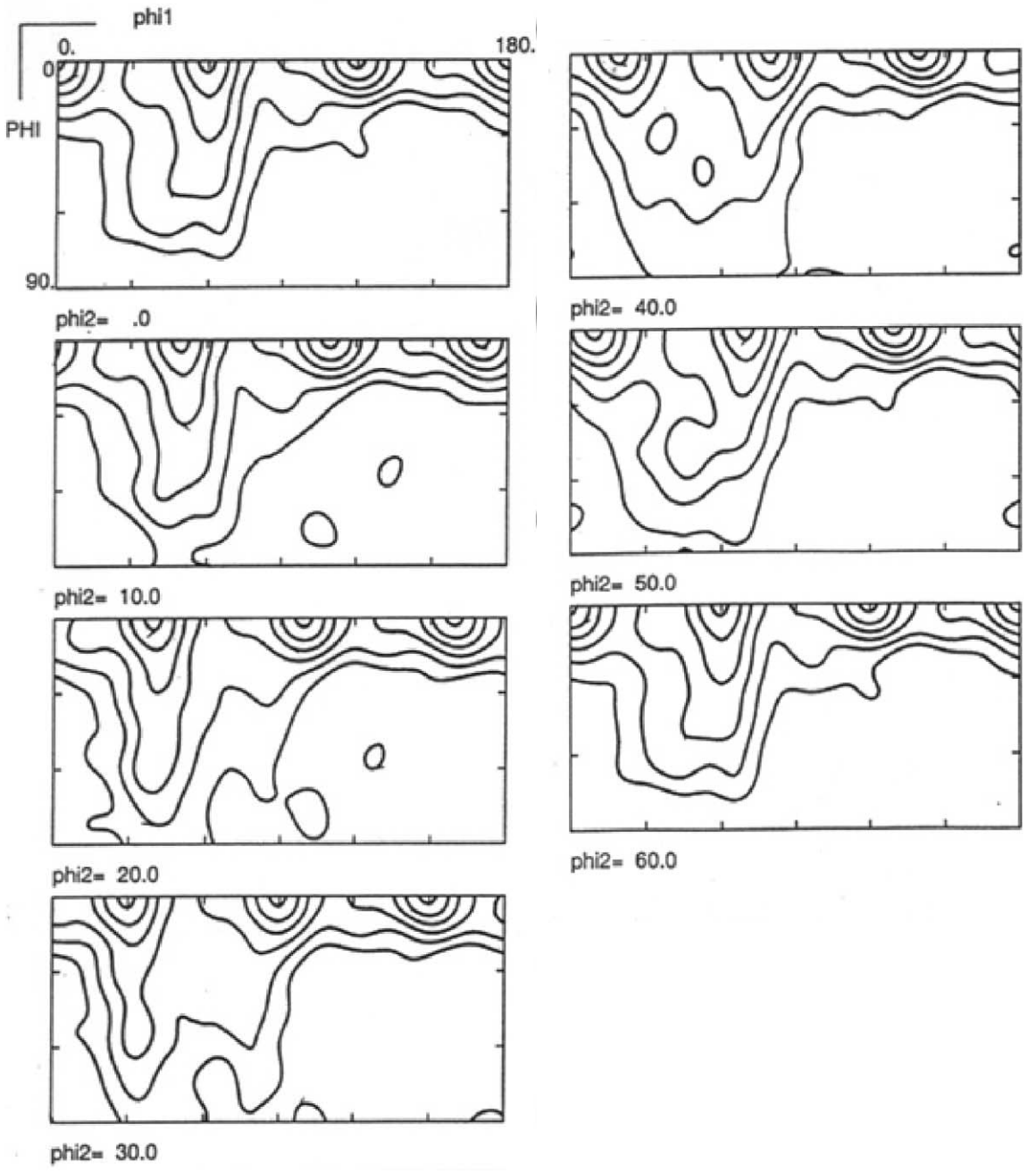

Fig. 7. ODF after a high temperature torsion test ($\varepsilon = 1.8$).

$\langle c + a \rangle$ slip is completely different. In this case, basal poles are distributed around the direction of greatest extension (Fig. 8(c)). When the pyramidal $\langle a \rangle$ slip is the active deformation mode, no significant differences compared to basal slip results can be observed (Fig. 8(d)).

The comparison of these results with the experimental pole figures allows us to choose the best combination of deformation modes and their CRSS to reproduce the experimental textures. In our case, prismatic and basal slip must be the most active deformation modes. On the other hand, pyramidal $\langle c + a \rangle$ slip must present a low activity mode and pyramidal $\langle a \rangle$ slip does not seem to introduce any significant change in the pole figures. The selected CRSS values are thus listed in Table 1.

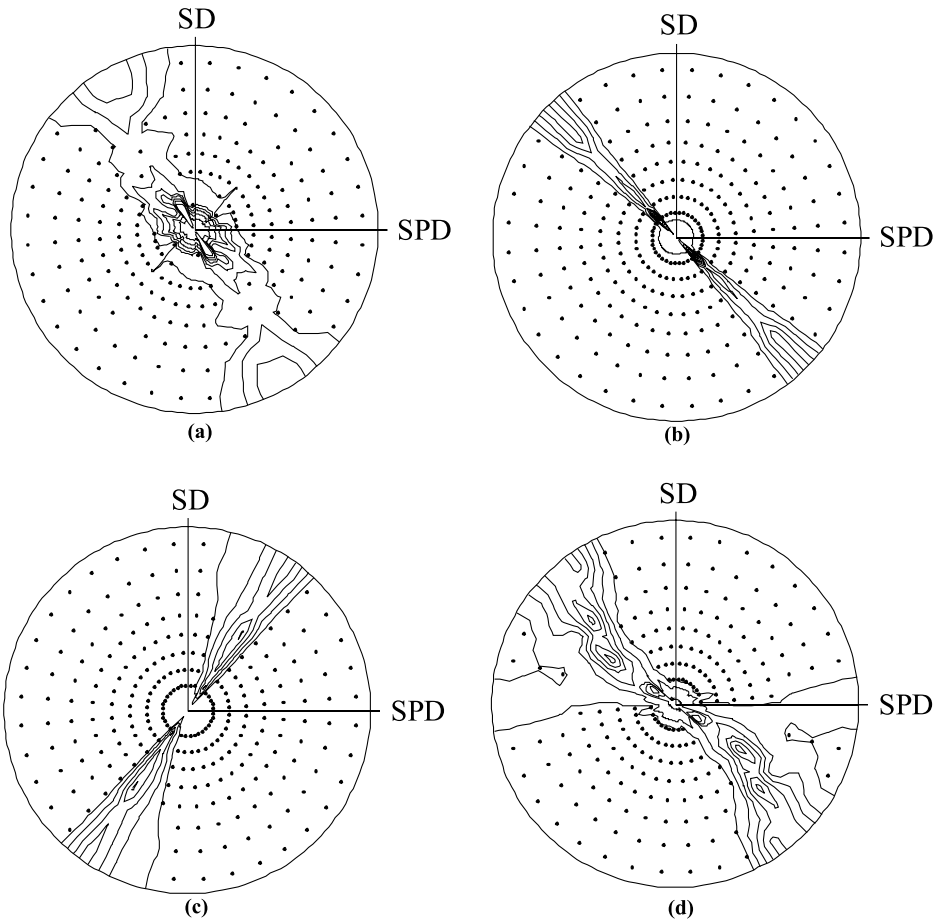

Fig. 8. Predicted (0 0 0 2) pole figures considering as deformation modes: (a) prismatic $\langle a \rangle$ slip, (b) basal $\langle a \rangle$ slip, (c) pyramidal $\langle c + a \rangle$ slip, (d) pyramidal $\langle a \rangle$ slip.

Table 1
Slip modes and associated CRSS values (in units of τ_{pr}) for torsion texture predictions

Slip mode	CRSS
Prismatic $\langle a \rangle$ or $\{1\,0\,\bar{1}\,0\}\langle 1\,\bar{2}\,1\,0 \rangle$	$\tau_{pr} = 1.0$
Basal $\langle a \rangle$ or $(0\,0\,0\,1)$ $\langle 1\,\bar{2}\,1\,0 \rangle$	$\tau_{bas} = 4.0$
Pyramidal $\langle a \rangle$ or $\{1\,0\,\bar{1}\,1\}\langle 1\,\bar{2}\,1\,0 \rangle$	$\tau_{pyr\langle a \rangle} = 2.0$
Pyramidal $\langle c + a \rangle$ or $\{1\,0\,\bar{1}\,1\}\langle 1\,1\,\bar{2}\,3 \rangle$	$\tau_{pyr\langle c+a \rangle} = 8.0$

4.2. Texture predictions and discussion

The predictions, which are shown below, are performed with a set of initially random orientations, since they were found to be very close to the ones obtained with the measured initial texture. This result could indicate that, like in rolling, the effect of the initial texture is erased at high strains.

For a strain equal to 0.8, it can be observed that the predicted (0 0 0 2) pole figure reproduces the approximate experimental fiber having its axis around the (+) direction (Fig. 9(a)). But, instead of having a single reinforcement (plus symmetrical) along the line of the $\langle c \rangle$ axes located at 30° from RD, we see three maximums at 0°, 20° and 90° from RD. The main orientation is clearly the orientation (30°, 90°, 20°), as seen from the $\{1\,0\,\bar{1}\,0\}$ pole figure (Fig. 9(b)).

When deformation increases ($\varepsilon = 1.8$, Fig. 10(a)), the central reinforcement of (0 0 0 2) pole figure is correctly predicted. But a second reinforcement is also clearly visible at around 50° from RD (compared to the previous figure, the maximum located at the periphery of the $\{0\,0\,0\,2\}$ pole figure has been shifted towards the center).

Predicted $\{1\,0\,\bar{1}\,0\}$ pole figures look qualitatively similar for both strains (Figs. 9(b) and 10(b)). As in the experimental pole figures, a reinforcement of pole densities around the (+) direction can be observed. Two other reinforcements are also predicted (one in the axial direction and the other at 30° from this direction), which are associated with the orientation having a $\langle c \rangle$ axis

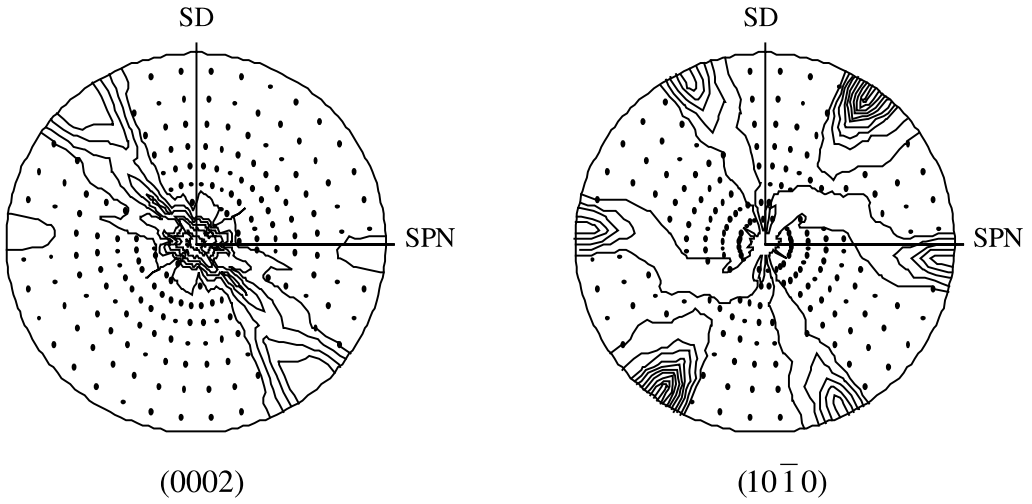

Fig. 9. Predicted (0 0 0 2) and (1 0 $\bar{1}$ 0) pole figures after a high temperature torsion deformation $\varepsilon = 0.8$. Active slip modes: prismatic and basal $\langle a \rangle$ and pyramidal $\langle c + a \rangle$.

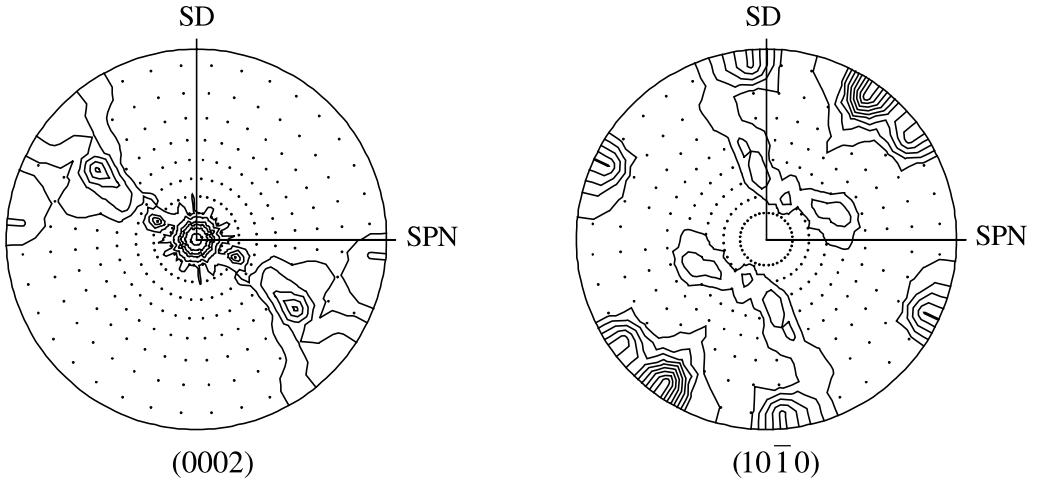

Fig. 10. Predicted (0 0 0 2) and (1 0 $\bar{1}$ 0) pole figures for a torsion effective deformation $\varepsilon = 1.8$. Active slip modes: prismatic and basal $\langle a \rangle$ and pyramidal $\langle c + a \rangle$.

along RD. No other combination of CRSS values could be found to give a better agreement with experimental textures.

Table 2 presents the relative activity of the different deformation modes for the initial deformation stage ($\varepsilon = 0.02$), for $\varepsilon = 0.8$ and $\varepsilon = 1.8$. As in the case of rolling textures simulations, the VPSC model favors the activation of prismatic and basal slip. A low activity of pyramidal $\langle c + a \rangle$ slip (lower than 5% of the total) can also be observed. At low and moderate strains ($\varepsilon = 0.02$ and $\varepsilon = 0.8$), variations in the activities of the deformation modes are not significant, being prismatic slip the main deformation mode. The equivalent Von Mises stress–strain curve corresponding to the material is presented in Fig. 11. It puts in evidence the effects of textural hardening. It can be observed that this effect is not significant (around 5% of the stress mean value). For large deformations, stress values can be considered as constant (or even to go down smoothly). This fact is of

Table 2
Calculated relative activities

Activity			
ε	pr$\langle a \rangle$ (%)	$b\langle a \rangle$ (%)	pyr$\langle c + a \rangle$ (%)
0.02	83	17	0
0.8	80	17	3
1.8	84	14	2

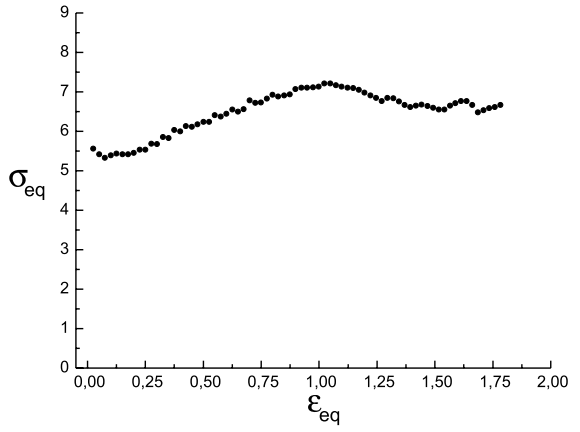

Fig. 11. Simulated equivalent strain–stress curve for the torsion test.

course associated with the relative texture stability with deformation.

The possible effect of the pyramidal $\langle a \rangle$ slip on texture generation was also studied. Simulations were thus performed by still considerably lowering the value of the CRSS for these slip systems (i.e., from 4 to 2). The obtained results indicate that there are no significant differences with predicted textures obtained considering only prismatic $\langle a \rangle$, basal $\langle a \rangle$ and pyramidal $\langle c + a \rangle$ slip as deformation modes. Then, we believe that the addition of the pyramidal $\langle a \rangle$ slip is not justified in terms of the texture description.

5. Conclusions

Texture analysis using experimental X-rays pole figures and the further calculation of the Orientation Distribution Function allow us to obtain a good description of texture components and their evolution during high temperature torsion tests in Zr.

Comparison between experimental and predicted textures put in evidence that the VPSC model can reproduce part of the experimental features only. In particular, the model does not allow us to get in the present case the same precision as the one obtained for the simulation of the room temperature rolling textures in hcp materials or of the torsion textures in cubic materials. This could be due to the incompatibility of the model to take into account, in its present version, the possible effects of dynamic recovery (i.e., thermal activation of cross-slip and climb mechanisms as well as the formation of polygonized grains), as usually visible at high temperature.

Basal $\langle a \rangle$ and prismatic $\langle a \rangle$ slip modes are necessary to reproduce the two main (0 0 0 2) poles density maxima located around radial direction and along the greatest compression direction. When torsion deformation increases ($\varepsilon = 1.8$) the effect of $\langle a \rangle$ basal slip allows a rotation of the $\langle c \rangle$ axes towards the axial direction. Then, we believe that $\langle a \rangle$ basal slip activity might decrease with deformation compared to $\langle a \rangle$ prismatic slip activity. On the other hand, the activity of pyramidal $\langle c + a \rangle$ slip must remain quite low in order to prevent the development of any texture component along the direction of greatest extension.

A more detailed study, considering results of detailed microstructural analyses of the torsion tests, including in situ studies using EBSD techniques in a SEM, could give us more detailed information about the existence of dynamic recovery and the activation of deformation modes in grains during process.

References

[1] C. Rossard, Mise en forme des métaux et alliages, CNRS, Paris, 1976.
[2] P. Van Houtte, Acta Metall. 26 (1978) 598.
[3] G. Canova, U. Kocks, J.J. Jonas, Acta Metall. 32 (1984) 211.
[4] P. Van Houtte, E. Aernoudt, K. Sekine, in: Proceedings of 6th International Conference on Textures of Materials, Tokyo, Japan, September 28–October 3, 1981, Nagashima, Tokyo, 1981.
[5] K. Sekine, P. Van Houtte, G. Sevillano and E. Aernoudt, in: Proceedings of 6th International Conference on Textures of Materials, Tokyo, Japan, September 28–October 3, 1981, Nagashima, Tokyo, 1981.
[6] F. Montheillet, M. Cohen, J.J. Jonas, Acta Metall. 32 (1984) 2077.
[7] F. Montheillet, in: Proceedings of 24th Colloque de Métallurgie, Saclay, France, June 1981, INSTM, 1981.
[8] W. Backofen, B. Hundy, Trans. AIME 197 (1953) 61.
[9] J. Baczinski, J.J. Jonas, Acta Metall. 44 (1996) 4273.
[10] Swift, Engineering 163 (1947) 253.
[11] F. Montheillet, P. Gilormini, J.J. Jonas, Acta Metall. 33 (1985) 705.
[12] L.S. Toth, J.J. Jonas, P. Gilormini, B. Bacroix, Int. J. Plasticity 6 (1990) 83.
[13] A. Pochettino, P. Sánchez, R. Lebensohn, C. Tomé, Mater. Sci. Forum 157–162 (1994) 835.
[14] P. Sánchez, R. Lebensohn, M. Gonzalez, A. Pochettino, in: S. Andersen, J. Bilde-Sorensen, T. Lorentz, O. Pedersen, N. Sorensen (Eds.), Proceedings of 15th RISØ International Symposium on Materials Science, Roskilde, Denmark, September 1994, Roskilde, 1994.
[15] R. Lebensohn, P. Sánchez, A. Pochettino, Scripta Metall. 30 (1994) 481.
[16] H.J. Bunge, Texture Analysis in Materials Science. Mathematical Methods, Butterworths, London, 1982.
[17] A. Vadon, PhD thesis, Metz University, 1981.
[18] R. Williams, Trans. AIME 224 (1962) 129.
[19] P. Gilormini, P. Roudier, P. Rougée, C. R. Acad. Sci. Paris I 136 (1993) 1659.

[20] B. Bacroix, Z. Hu, Metall. Mater. Trans. 26A (1995) 601.
[21] R. Lebensohn, C. Tomé, Acta Metall. 41 (1993) 2611.
[22] R. Brenner, J. Bechade, O. Castelnau, B. Bacroix, in: D. Miannay, et al. (Eds.), Proceedings of EUROMAT 2000, Tours, France, November 2000, Elsevier, Amsterdam, 2000.